Vibrational Population Relaxation of the −N═C═N− Antisymmetric Stretching Mode of Carbodiimide Studied by the Infrared Transient Grating Method

Hiroaki Maekawa,[†] Kaoru Ohta,[‡] and Keisuke Tominaga*[,†,‡,§]

Graduate School of Science and Technology, CREST, JST, and Molecular Photoscience Research Center, Kobe University, Nada, Kobe 657-8501, Japan

Received: May 18, 2004; In Final Form: August 5, 2004

Vibrational dynamics of the carbodiimide (−N═C═N−) antisymmetric stretching mode of dicyclohexylcarbodiimide (DCCD) in carbon tetrachloride and *N*,*N*-dimethylformamide have been investigated by the transient grating method. The magic angle transient grating experiment reveals that the population relaxation of the $v = 1$ state occurs nonexponentially and is reproduced well by a biexponential function with time constants of 200−300 fs and 1.4−1.5 ps with almost equal amplitudes. A time scale of the orientation relaxation is longer than a few picoseconds. Frequency-resolved transient grating measurement has shown that this nonexponential behavior is interpreted by a model of rapid population distribution to other modes and irreversible relaxation from these modes.

I. Introduction

It is important to investigate microscopic aspects of solutions, such as solute−solvent interactions, dynamical fluctuations, and local structures of solvent, because they play crucial roles in chemical and biological reactions in liquids. Vibrational populational relaxation is related to dissipation of an excess energy in condensed phases and has been extensively investigated by, for example, infrared (IR) pump−probe technique.[1−6] Vibrational population relaxation is also an important quantity to test a theoretical model on the interaction between a solute and solvent. A theoretical framework of vibrational relaxation has been established and reviewed in many places.[7,8] Some experimental results on simple systems such as diatomic molecules and ions have been discussed in terms of analytical theories, such as hydrodynamics models, and computer simulation.

For a polyatomic molecule, there are two processes which contribute to vibrational population relaxation, energy distribution between the initially excited mode and other modes coupled anharmonically to it (intramolecular vibrational energy redistribution) and energy dissipation toward the surrounding solvent molecules (vibrational cooling). Recently, Hochstrasser and coworkers reported ultrafast, nonexponential vibrational population relaxation for some polyatomic molecules.[9−11] The fast-decaying component has a time constant of a subpicosecond, and the slow one has a few picoseconds time scale. The fast component of the relaxation is much faster than most of the vibrational relaxation times reported previously, where vibrational energy is directly transferred to intermolecular degrees of freedom of the surroundings. For such a fast process, intramolecular interaction such as anharmonic coupling must play an important role. Furthermore, intermolecular interactions may strongly affect the intramolecular process, like solvent-assisted intramolecular vibrational relaxation, in which vibrational energy flows among solute intramolecular modes by conserving the total energy with solvent low-frequency vibrational, rotational, and translational energy.

* Corresponding author. E-mail: tominaga@kobe-u.ac.jp.
[†] Graduate School of Science and Technology.
[‡] CREST, JST.
[§] Molecular Photoscience Research Center.

SCHEME 1

$$-N{=}C{=}N- \leftrightarrow -\ddot{N}{=}C^{+}{-}N^{-}- \leftrightarrow -N^{+}{\equiv}C{-}N^{-}-$$

It is also necessary to obtain detailed information on vibrational population relaxation to understand the vibrational dephasing process, particularly by means of nonlinear-infrared spectroscopy such as a photon echo method.[10−12] That is especially important when the time scale of the population relaxation is similar to that of the dephasing. Furthermore, some vibrational modes exhibit nonexponential population relaxation on a similar time scale to that of the vibrational dephasing that makes analysis complicated. The population relaxation on the $v = 2$ state should also be taken into account to interpret the signal observed in nonlinear-IR spectroscopy. In some cases, the lifetime of the $v = 2$ state is reasonably described by the harmonic approximation, which is half of the lifetime of the $v = 1$ state. However, it is experimentally confirmed that this is not always the case, especially for polyatomic molecules.[10,13]

In this study we have applied the IR transient grating method to the carbodiimide (−N═C═N−) antisymmetric stretching mode of dicyclohexylcarbodiimide (DCCD). We employed the transient grating method instead of the conventional pump−probe method to study vibrational dynamics of the mode. One advantage of using the transient grating method is that we can switch to the photon echo experiment to study vibrational dephasing without any major change in the experimental configuration. The −N═C═N− antisymmetric stretching mode consists of motions of the three atoms connected with its adjacent atom by a cumulative double bond.[14] It is extensively known that conversion among three structures with different charge distributions and covalent bonds is considered to take place (Scheme 1).

Carbodiimides are important compounds as versatile reagents in organic and biochemical synthesis.[15,16] Most of the reactions of carbodiimides involve nucleophilic attack to the carbon atom, and the nucleophilic addition of water to DCCD is widely used for dehydration.[17−19] In the past, the equilibrium structure and physical properties of carbodiimides were studied theoretically and experimentally;[20−22] however, dynamical aspects of the

10.1021/jp047870d CCC: $27.50
Published on Web 10/07/2004

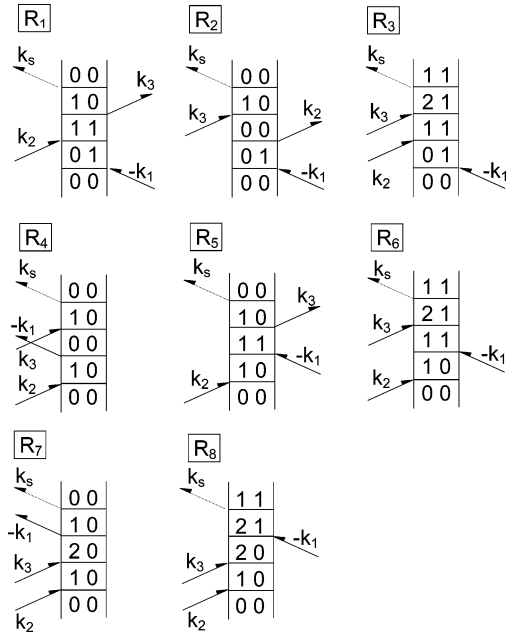

Figure 1. Feynman diagrams of the eight pathways contributing to the third-order nonlinear polarization with a phase-matched direction of $-\mathbf{k}_1 + \mathbf{k}_2 + \mathbf{k}_3$.

carbodiimides were not investigated though such information is important to understand the reactivity of the molecules. The conversion among the three structures will induce frequency fluctuations of the −N═C═N− mode, and, therefore, investigation on the vibrational dynamics of this mode is a good target for nonlinear-IR spectroscopy. This paper is composed as follows. After a brief explanation of the theory on nonlinear-IR spectroscopy in section II, details of the experimental setup are described in section III, and experimental results and discussion of the IR transient grating are given in section IV.

II. Theory

The detailed theoretical formalism of nonlinear-IR spectroscopy is described in the literature.[23] The third-order nonlinear polarization $P^{(3)}(t;\tau,T)$ is expressed as a sum of nonlinear response functions convoluted with the electric fields E of the three IR pulses

$$P^{(3)}(t;\tau,T) = \left(\frac{i}{\hbar}\right)^3 \int_0^\infty \mathrm{d}t_3 \int_0^\infty \mathrm{d}t_2 \int_0^\infty \mathrm{d}t_1 \sum_i R_i(t_1,t_2,t_3) \times E(t-t_3)E(t+T-t_3-t_2)E(t+T+\tau-t_3-t_2-t_1) \quad (1)$$

For the nonlinear polarization with a wavevector of $-\mathbf{k}_1 + \mathbf{k}_2 + \mathbf{k}_3$, there are eight Feynman diagrams to be considered (Figure 1). The response function corresponding to each diagram is expressed in terms of the time correlation function of fluctuations of the transition frequency between the $v = 0$ and 1 states, $\langle \delta\omega_{10}(t)\ \delta\omega_{10}(0)\rangle$, provided that the anharmonicity of the vibrational mode has no fluctuations, that is $\delta\omega_{21}(t) = \delta\omega_{10}(t)$. For example, the response functions for the diagrams R_1 and R_2 are written as follows,[23]

$$R_1(t_1,t_2,t_3) = R_2(t_1,t_2,t_3) = |\mu_{10}|^4 \mathrm{e}^{i\omega_{10}(t_1-t_3)} \exp[-g(t_1) + g(t_2) - g(t_3) - g(t_1+t_2) - g(t_2+t_3) + g(t_1+t_2+t_3)] \quad (2)$$

where a line shape function $g(t)$ is given by

$$g(t) = \int_0^t \mathrm{d}\tau_2 \int_0^{\tau_2} \mathrm{d}\tau_1 \langle \delta\omega_{10}(\tau_1)\delta\omega_{10}(0)\rangle \quad (3)$$

In the above equations, μ_{10} and μ_{21} are the transition moments between the $v = 0$ and 1 states, and the $v = 1$ and 2 states, respectively, and under a harmonic approximation for the transition moment, the relation of $\mu_{21} = \sqrt{2}\mu_{10}$ is valid. The observed time-integrated signal $S(\tau,T)$ is represented as follows,

$$S(\tau,T) = \int_{-\infty}^{\infty} |P^{(3)}(t;\tau,T)|^2 \,\mathrm{d}t \quad (4)$$

Effects of the orientational and population relaxation are included in terms of phenomenological decay components, and the response functions are modified by additional decay functions for the orientational and population relaxation.[10,11] For example, when the population relaxation can be described by a single-exponential function, its effects on the vibrational dephasing are taken into account through a factor of $\exp(-t/2T_1^{(1)})$ for the vibrational dephasing between the $v = 0$ and 1 states, where $T_1^{(1)}$ is a lifetime of the $v = 1$ state. Additionally, for a harmonic oscillator linearly coupled with a heat bath, the population relaxation time is inversely proportional to the vibrational quantum number. Therefore, a lifetime of the $v = 2$ state $T_1^{(2)}$ is half of $T_1^{(1)}$, and the contribution of the population relaxation to dephasing between the $v = 1$ and 2 states is expressed by a factor of $\exp(-t/2T_1^{(1)} - t/2T_1^{(2)})$. When the population relaxation is described by a biexponential function, its contribution to the response function is considered phenomenologically by the time-dependent rate constant.[11] The time-dependent rate constant of the population relaxation of the $v = 1$ state $k_1(t)$ is expressed as,

$$k_1(t) = -\frac{\mathrm{d}P(t)/\mathrm{d}t}{P(t)} \quad (5)$$

where $P(t)$ is the quantity proportional to the population and determined from the transient grating experiment. The rate of the $v = 2$ state $k_2(t)$ is assumed to be twice as large as $k_1(t)$, from an analogue of the harmonic approximation for a single-exponential relaxation. Within this treatment of the nonexponential population relaxation, its contribution to vibrational dephasing between the $v = 1$ and 0 states and the $v = 2$ and 1 states is described by a factor of $\exp(-1/2 \int_0^t k_1(t')\,\mathrm{d}t')$ and $\exp\{-1/2(\int_0^t k_1(t')\,\mathrm{d}t' + \int_0^t k_2(t')\,\mathrm{d}t')\}$, respectively.

III. Experimental Section

The laser system used for nonlinear-IR experiments was described previously.[24] Briefly, short IR pulses are generated by difference frequency mixing the signal and idler pulses from an optical parametric amplifier pumped by an output of the Ti:Sapphire regenerative amplifier. A $AgGaS_2$ crystal (thickness of 1.75 mm) was used for the difference frequency mixing, and the near-IR pulses with wavelengths of about 1370 and 1920 nm were incident on it noncollinearly. The IR pulse has a Gaussian-shaped spectrum with a full width at half-maximum (fwhm) of about 120 cm^{-1} at a central frequency of 2120 cm^{-1} (Figure 2a). The IR pulse with a pulse energy of about 4 μJ/pulse was generated into a different direction from the residual near-IR pulses and picked up without any additional optics such as a prism pair or a long wavelength pass filter. For compressing the IR pulses, a semiconductor window such a silicon or germanium was inserted into an optical path.[24,25] Silicon and germanium have group velocity dispersion coefficients with an opposite sign to that of optical materials such as CaF_2 in the IR region. In our system, a silicon window with a thickness of 2 mm and antireflection coating on both sides was set at the output of the difference frequency generator. A pulse width of the

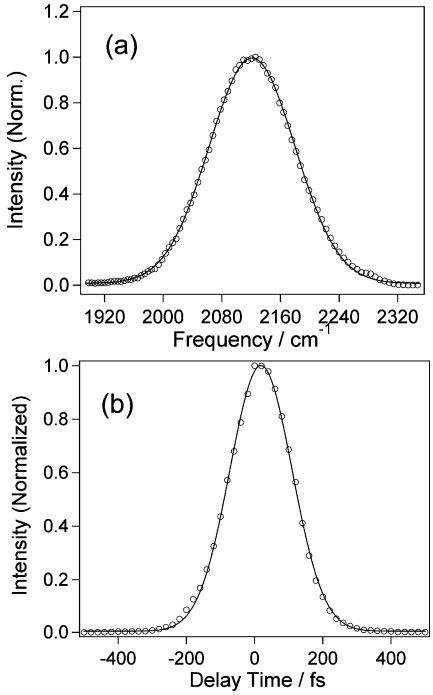

Figure 2. (a) A spectrum of the infrared pulse (circle). The solid line is a result of the fitting with a Gaussian function. A spectral width is estimated to be about 120 cm^{-1}. (b) The autocorrelation function of the infrared pulse (circle). The solid line is a result of the fitting with a Gaussian function. A pulse width is estimated to be about 150 fs.

compressed IR pulse was estimated to be about 150 fs from noncollinear autocorrelation measurement with use of a $AgGaS_2$ crystal (thickness of 0.5 mm) (Figure 2b).

The IR pulse was collimated by using two curved mirrors with a radius of curvature of 600 and 400 mm and split into three parts by two CaF_2 beam splitters. Each pulse was delivered into a retro-reflector mounted on a computer-controlled mechanical stage. In the experiment, τ and T denote the time interval between pulse 1 (denoted by its wavevector $\mathbf{k}_1$) and pulse 2 ($\mathbf{k}_2$), pulse 2 and pulse 3 ($\mathbf{k}_3$), respectively. The origin of the delay time was determined within an error of a few tens of femtoseconds by an autocorrelation method. The three pulses were aligned in a boxcar geometry and focused into a sample cell with an off-axis parabolic mirror (an effective focal length of 101.6 mm). A signal generated into a phase-matching direction of $-\mathbf{k}_1 + \mathbf{k}_2 + \mathbf{k}_3$ was collimated with another parabolic mirror and separated spatially from the residual pump pulses. The signal was detected by a liquid nitrogen cooled indium antimonide (InSb) detector and processed by a boxcar gated integrator and a lock-in amplifier. The $\mathbf{k}_1$ pulse was synchronously chopped at half the repetition rate of the regenerative amplifier.

For the transient grating measurements, the $\mathbf{k}_1$ and $\mathbf{k}_2$ pulses were incident into the sample simultaneously ($\tau = 0$ fs), and the diffracted signal of the delayed $\mathbf{k}_3$ pulse to the phase matched direction of $-\mathbf{k}_1 + \mathbf{k}_2 + \mathbf{k}_3$ was detected as a function of the delay time T. To separate populational dynamics from orientational relaxation, a polarization direction of the probe pulse was set at a magic angle to that of the pump pulses by using a wire-grid polarizer with an extinction coefficient of 1:200, and an analyzer set to the same angle was placed in front of the InSb detector. The signal was dispersed in a monochromator to measure a spectrum of the transient grating signal. A slit width of the monochromator was set to 250 μm to achieve a frequency resolution of 1.8 cm^{-1}. The dispersed signal was detected with a liquid nitrogen cooled InSb detector.

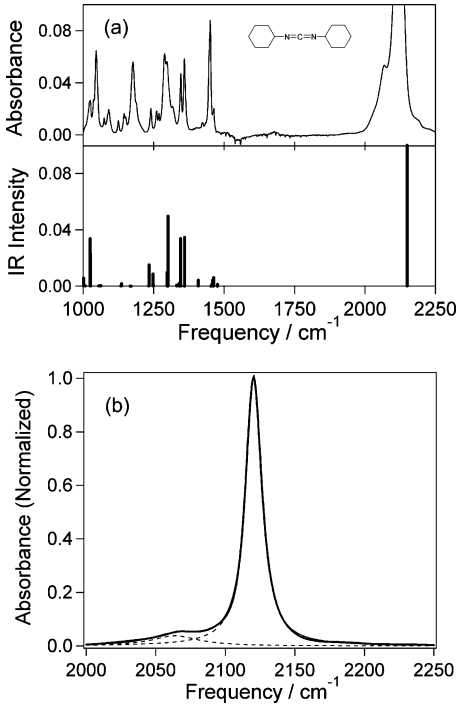

Figure 3. (a) An infrared absorption spectrum of dicyclohexylcarbodiimide (DCCD) in CCl_4 solution. The absorbance is normalized by the peak intensity of the −N═C═N− antisymmetric stretching mode (2120 cm^{-1}). There is an absorption band due to the solvent at around 750 cm^{-1}. The IR intensities obtained by the DFT calculation are represented by stick diagrams. (b) IR absorption band for the −N═C═N− antisymmetric stretching mode (thick solid line). The spectrum is simulated by a sum of two Lorentzian functions. Each component is shown by a dashed line, and the sum of them is indicated by a thin solid line. Optimized parameters are summarized in Table 1.

Samples (DCCD (Aldrich), CCl_4 and DMF (Wako)) were used without further purification. The sample solution was retained in a sample cell with a spacer (an optical path length of 200 μm) between CaF_2 windows (a thickness of 3 mm), and the concentration of the sample solution was adjusted to 35 mM so that the maximum optical density at the excitation wavelength was about 1.0. An IR absorption spectrum of the DCCD solution was measured by a FT-IR spectrometer (PERKIN ELMER, Spectrum1000). A polarized and depolarized Raman spectrum was measured with the 514.5-nm line from a CW Ar^+ ion laser (Spectra Physics, BeamLok). All measurements were performed at ambient temperature (22 ± 1 °C).

IV. Results and Discussion

Vibrational Spectra and ab Initio Calculation. A FT-IR spectrum of DCCD is shown in Figure 3. The band of the −N═C═N− antisymmetric stretching mode has a maximum optical density at 2120 cm^{-1} in CCl_4 and 2118 cm^{-1} in DMF with a molar absorption coefficient ϵ of about 1430 M^{-1} cm^{-1}.[26,27] A weak band is also observed at the lower frequency side of the −N═C═N− band. The FT-IR spectrum observed for the CCl_4 solution is fitted by a sum of two Lorentzian functions (dashed lines in Figure 3b), and the weak band has a peak at 2068 cm^{-1} and a bandwidth of about 42 cm^{-1}. The results of the FT-IR spectrum measurements are summarized in Table 1. In the Raman spectra from 1000 to 1500 cm^{-1}, there are several polarized bands at around 1010, 1146, 1407, and 1463 cm^{-1}. The other bands have almost the same peak frequency (within 2 cm^{-1}) and a bandwidth in the parallel and perpendicular component of the Raman spectrum.

TABLE 1: Parameters for the FT-IR Spectrum of Dicyclohexylcarbodiimide

solvent	CCl_4	DMF
(a) −N═C═N− mode		
peak frequency/cm^{-1}	2120	2118
line width (fwhm)/cm^{-1}	15.2	13.8
(b) weak band at lower frequency side		
peak frequency/cm^{-1}	2064	2063
line width (fwhm)/cm^{-1}	41.4	42.0
intensity ratio (weak band/−N═C═N− mode)	0.111	0.104

TABLE 2: Summary of FT-IR and Raman Spectra Measurements and the DFT Calculation for Dicyclohexylcarbodiimide (in cm^{-1})

IR		Raman		
exptl	calcd	exptl	calcd	assignment
		1010 (p)[a]	1008 (p)	CH_2 wagging + CH bending
1025	1002			CH_2 wagging
		1028	1027	CH_2 wagging + CH bending
1046	1024			CH_2 wagging + CH bending
		1053	1055	CH_2 twisting + CH bending
1075		1075		C−N stretching[b]
1091				
1125		1122		
1145	1135			CH_2 rocking
		1147 (p)	1133 (p)	CH_2 rocking
1151				
1177				C−C skeletal [b]
1188				
		1190	1170	CH_2 wagging + CH_2 twisting
1240	1233	1244	1233	CH_2 twisting + CH bending
1261	1248	1262	1248	CH_2 twisting + CH bending
1269				
1289	1297	1305	1297	CH_2 wagging + CH bending
1297	1301			CH_2 wagging + CH_2 twisting
1317				
1347	1347	1346	1347	CH_2 wagging + CH bending
1359	1359	1361	1359	CH_2 wagging + CH bending
		1407 (p)	1408 (p)	−N═C═N− symmetric stretching
1451	1456	1446	1453	CH_2 scissoring
1464	1463	1462 (p)	1463 (p)	CH_2 scissoring
2118	2150			−N═C═N− antisymmetric stretching

[a] (p) denotes a polarized band. [b] Assignment in ref 26.

The molecular structure and the IR and Raman spectra of DCCD are calculated with the density functional theory (DFT) method at the level of B3LYP/6-31G(d) with the GAUSSIAN 03W package.[28] From the X-ray structure analysis, it was reported that the N−C−N angle of carbodiimide compounds is slightly deviated from 180°.[16] The optimized structure of DCCD in our calculation shows the angle of 171.8°. Vibrational frequencies scaled by an empirical factor of 0.9613 are tabulated in Table 2, along with the experimental results, and calculated IR intensities are represented by a stick diagram in Figure 3a. Almost all the vibrational bands are reproduced by the calculation, except for several IR-active bands around 1100 cm^{-1}. The vibrational spectra are congested due to the CH_2 bending modes in the frequency region from 1000 to 1500 cm^{-1}, and, therefore, the complete assignment of the vibrational bands is not a simple task. However, the band at 1407 cm^{-1} can be assigned to the −N═C═N− symmetric stretching mode from the results of the calculation and the Raman spectrum measurement, which may play an important role in a vibrational relaxation process of the −N═C═N− antisymmetric stretching discussed later.

Transient Grating Signal. Figure 4 shows a transient grating signal at the magic angle condition. To examine a contribution from a higher order nonlinear polarization, we investigated a power dependence of the observed signal. The total intensity of the IR pulse is reduced to 55% of the original one by a CaF_2 beam splitter. The observed signal has an intensity ratio of 0.170 compared to that measured without decreasing the intensity, which is within experimental error from the expected value of 0.166 (Figure 5a). We have also confirmed that no signals from CaF_2 windows or solvent molecules are detected under the present condition.

The transient grating signal, which was observed at the parallel polarization condition, shows a similar decay to that at the magic angle condition (Figure 5b), and it is conceivable that a reorientational relaxation of DCCD in CCl_4 occurs on a time scale longer than a few picoseconds. In measurements with other techniques such as optical Kerr effect spectroscopy and

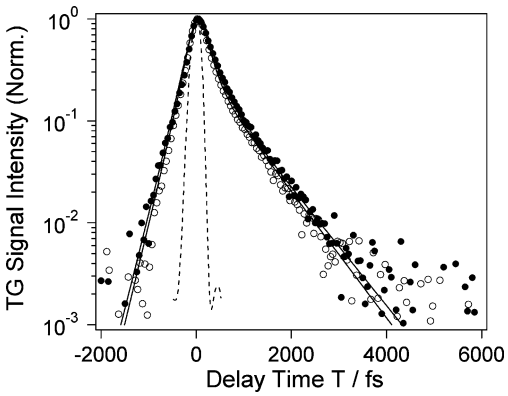

Figure 4. Transient grating signals of the −N═C═N− antisymmetric stretching mode of dicyclohexylcarbodiimide in CCl_4 (white circle) and *N*,*N*-dimethylformamide (black circle). Solid lines represent biexponential fits to the experimental data. The autocorrelation is shown by a dashed line.

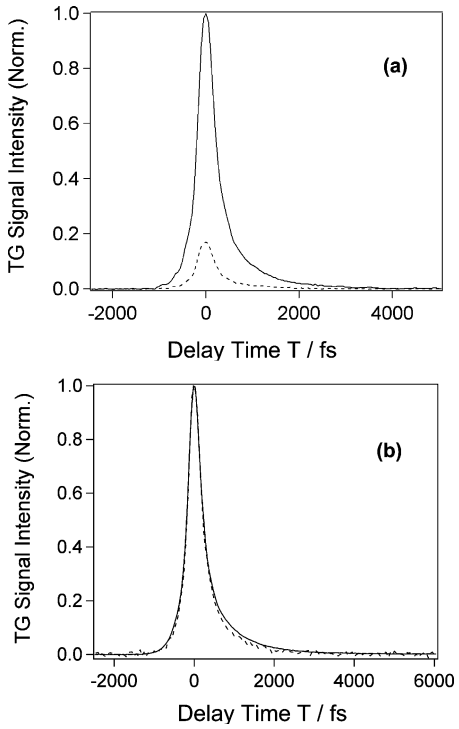

Figure 5. (a) Laser power dependence of the transient grating signal of the −N═C═N− antisymmetric stretching mode of dicyclohexylcarbodiimide in CCl_4. The laser power is reduced to 55% of the original value. (b) Polarization dependence of the transient grating signal. The signals measured with the probe pulse polarized to the parallel and to the magic angle direction with respect to the pump pulses are represented by solid and dashed lines, respectively.

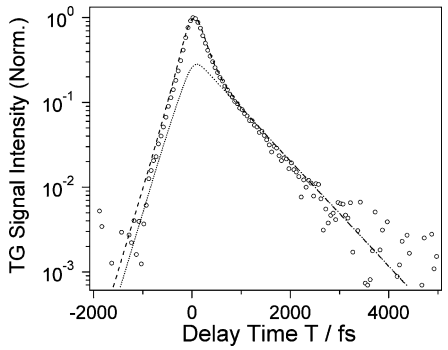

Figure 6. Transient grating signal of the −N═C═N− antisymmetric stretching mode of dicyclohexylcarbodiimide in CCl_4 (circles), and simulated results with only a slow component for the vibrational relaxation (dotted line) and with both a fast and slow components (dashed line).

fluorescence depolarization measurement, the reorientational relaxation of molecules with a similar size and mass in a nonviscous solvent occurs on a time scale of longer than 10 ps.[29] These results are consistent with our observation.

It should be noted that a state giving a band at 2068 cm^{-1} makes a negligibly small contribution to the observed signals. In the homodyne detected transient grating, the signal intensity is proportional to the forth power of the integrated absorption coefficient. From the fitting with a sum of two Lorentzian functions, the integrated absorption coefficient for the observed two bands is in an approximate ratio of 1:0.10 (Table 1). A predicted ratio of the signal intensity is $1:10^{-4}$, and, therefore, the excitation of the band at 2068 cm^{-1} makes a negligibly small contribution to the third-order nonlinear polarization. The contribution of coherence between the two modes is also expected to be small (order of $\sim 10^{-2}$). Therefore, it is not necessary to consider quantum pathways which include the interaction between the state giving the weak band and the electric field of the IR pulse.

The transient grating signals for the CCl_4 and DMF solutions show a nonexponential behavior: a rapid decay with a subpicosecond time scale followed by a slow decay with a picoseconds time scale. The signal can be fitted reasonably well with the square of the sum of two exponential functions. The time constants of the fast and slow decaying components in CCl_4 are 200 (54%) an 1400 fs (46%), respectively, and 300 (54%) and 1500 fs (46%), respectively, in DMF. An important question is whether the rapid decay reflects real vibrational dynamics or is due to a coherent artifact. When the pump and probe pulses are well separated in time, there are three quantum pathways contributing to the signal (R_1, R_2, and R_3 in Figure 1). However, there are eight time-orderings of the three radiation−matter interactions that can contribute to the signal when the pump and probe pulses overlaps in time (Figure 1). To investigate this point, we compare the temporal profile of the autocorrelation with the initial decay of the signal (Figure 4). It is apparent that the initial decay is much slower than the autocorrelation, showing that this is not due to the effect of the coherent artifact.

We further simulated the signal to confirm that the rapid decay corresponds to the vibratioinal dynamics. The transient grating signal was calculated according to eqs 1−4 by convoluting all of the eight response functions represented in Figure 1 with the three electric fields of IR pulses with a duration of 150 fs. Figure 6 compares the experimental data and theoretical calculation. The dotted line is the calculated transient grating signal with a single component for the vibrational relaxation.

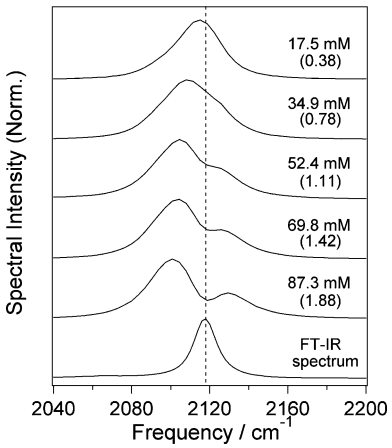

Figure 7. Transient grating spectra of the −N═C═N− antisymmetric stretching mode of dicyclohexylcarbodiimide in *N*,*N*-dimethylformamide and its concentration dependence. The delay time *T* is 0 fs. The FT-IR spectrum is also shown. The maximum optical densities are shown in parentheses. The dashed line shows the peak of the FT-IR spectrum (2118 cm^{-1}).

We choose $T_1^{(1)}$ of 1.4 ps to reproduce the long time behavior ($T > 1.0$ ps) of the signal. As for the line shape function $g(t)$, an exponential form ($\Delta^2 \exp(-t/\tau)$) is used with a time constant τ of 0.3 ps and a preexponential factor Δ of 2.5 ps^{-1}. The parameters of $g(t)$ were chosen to reproduce the transient grating signal in the negative delay time whose time dependence is mainly determined by the vibrational dephasing. Since the vibrational frequency fluctuation is in the rapid modulation limit ($\Delta\tau < 1$), a dephasing time ($1/\Delta^2\tau$) is an important quantity to reproduce the signal. On the other hand, the dashed line is the calculated result with a fast component (200 fs, 54%) and a slow component (1.4 ps, 46%). From Figure 6 one can confirm that it is impossible to reproduce the signal trace without the fast decaying component. Therefore, we conclude that the fast decaying component represents the real vibrational dynamics.

Frequency-Resolved Transient Grating Signal. The transient grating method can differentiate dynamics of the $v = 0$ state from that of the $v = 1$ state by frequency-resolving the signal. Figure 1 shows the eight Feynman diagrams related to the signal detected in the $-\mathbf{k}_1 + \mathbf{k}_2 + \mathbf{k}_3$ direction. If the spectral width of the pulse is broader than anharmonicity, then the induced third-order nonlinear polarization has two frequency components ω_{10} and ω_{21} during the detection time *t*, where ω_{10} and ω_{21} is the transition frequency between the $v = 0$ and 1 states and that between the $v = 1$ and 2 states, respectively. In the spectrum of the transient grating signal, two spectral components with frequencies of ω_{10} and ω_{21} can be separated due to the anharmonicity. The decay of the spectral intensity at the lower frequency side indicates dynamics of the $v = 1$ state, because the induced polarization with a frequency of ω_{21} is generated by a quantum pathway whose diagonal state of a density matrix is only in the $v = 1$ state (diagrams of R_3 and R_6).

Figure 7 shows a spectrum of the transient grating signal for the DMF solution at $T = 0$ fs, and its concentration dependence. The concentrations are 17.5, 34.9, 53.4, 69.8, and 87.3 mM. The spectrum for the concentrated solution shows two peaks, and the peak at the higher frequency side (2130 cm^{-1}) is shifted by about 10 cm^{-1} from the peak position of the FT-IR spectrum. However, these two peaks appear not due to anharmonicity but due to reabsorption of the signal in the sample, as pointed out by Asplund et al.[30] At the lower concentrations the spectrum seems a single broad component with a peak shifted to a lower

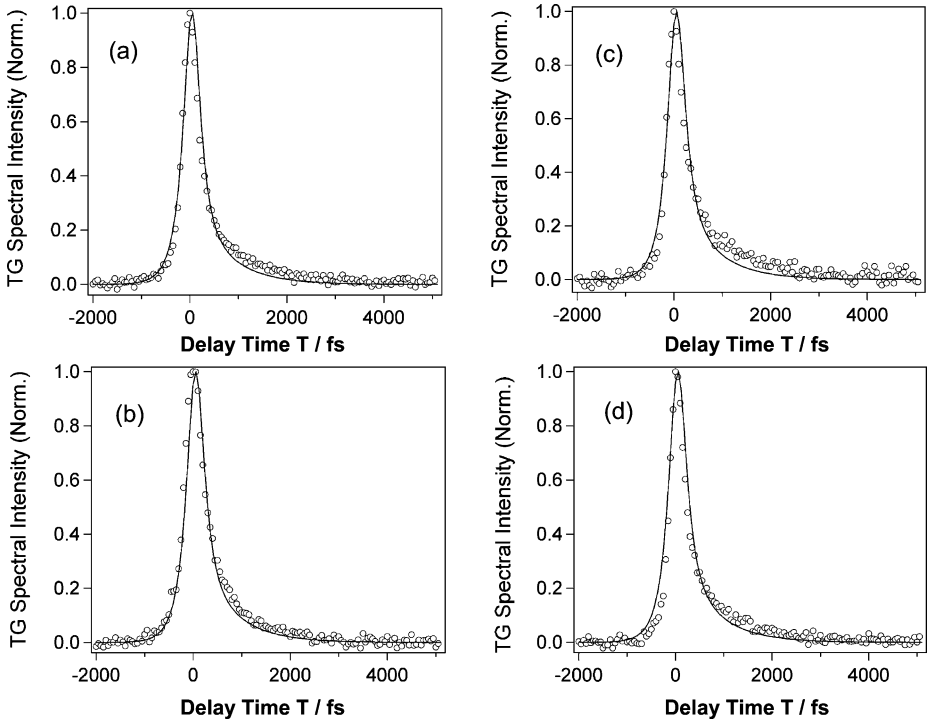

Figure 8. Frequency-resolved transient grating signals of the −N═C═N− antisymmetric stretching mode of dicyclohexylcarbodiimide in CCl_4 (circle) observed at a frequency of (a) 2087, (b) 2106, (c) 2119, and (d) 2131 cm^{-1}, respectively. The solid lines represent a signal calculated with parameters obtained by the simulation of the time-integrated transient grating signal (Figure 4).

frequency side and a broader line width. This is because the size of the anharmonicity is similar to that of the line width. To estimate the anharmonicity it is necessary to simulate the line shape of the frequency-resolved transient grating signals based on theoretical treatment for nonlinear-IR spectroscopy. The anharmonicity for the −N═C═N− mode is roughly estimated about 20−25 cm^{-1} from a preliminary simulation.[31]

The frequency-resolved transient grating signal observed at the frequency position of 2087, 2106, 2119, and 2131 cm^{-1} is shown in Figure 8 along with the fitting results. The fitting was performed with the same parameters obtained from the transient grating signal shown in Figure 4. The decay of the frequency-resolved transient grating signal is almost independent of the observed frequency. Especially, at 2087 cm^{-1} where a contribution of the fundamental transition to the signal may be negligible, the decay of the frequency-resolved transient grating signal is dominated by dynamics of the $v = 1$ state. From these results, the nonexponential behavior results from the population relaxation on the excited state.

Origin of the Nonexponential Decay. The results of the transient grating measurements indicate that the population relaxation of the $v = 1$ state proceeds nonexponentially. So far a nonexponential decay has been observed for vibrational population relaxation in several systems. Among them some of the vibrational modes show relaxation times ranging from subpicoseconds to several picoseconds. Hamm et al. reported that population relaxation of the amide I band of some peptides[9] and *N*-methylacetamide[10] shows a biexponential decay with time constants of subpicosecond and several picoseconds. They interpreted the results in terms of a model that the fast decaying component is due to specific Fermi resonances and the slow one results from relaxation of modes strongly coupled to the initially excited state. Lim and Hochstrasser observed a biexponential decay with similar time scales to those of the previous example for vibrational relaxation of the CO mode of acetic acid dimer.[11] As a source of the nonexponential dynamics they suggested that the solvent memory effects may play a role in vibrational dynamics in the regime where the rotational, vibrational, and dephasing times are all comparable.

SCHEME 2

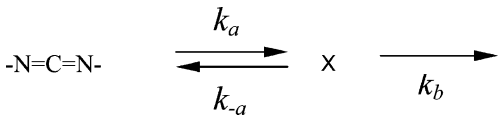

A possible explanation for the present case is that the nonexponential relaxation is due to an intramolecular process similar to the previous case. The time scale is too fast to be explained by direct energy transfer between the mode excited and the solvent. We here consider a mechanism that the excited population on the −N═C═N− antisymmetric stretching mode is rapidly distributed into other intramolecular vibrational modes prior to irreversible relaxation from these modes to lower frequency modes. The same mechanism was used to interpret population relaxation of the methyl stretching mode of methanol, in which rapid distribution of the excited population between the symmetric and antisymmetric methyl stretching modes is followed by vibrational energy relaxation to lower frequency modes.[4,32]

The mechanism with the rapid distribution and irreversible relaxation is expressed as Scheme 2, where X denotes the intermediate state, and k_i is the rate constant of each process. A schematic picture for this model is the following: the initial population in the $v = 1$ state prepared by a pump pulse proceeds population equilibration with a combination or overtone band, which is energetically close to the −N═C═N− antisymmetric stretching mode. There may be many vibrational bands near the fundamental of the combination or overtone band interacting with the −N═C═N− antisymmetric stretching mode, and the energy flow from the fundamental is rapid and irreversible. According to Scheme 2, the population on the $v = 1$ state of the −N═C═N− mode (represented by $p(t)$) decays biexpo-

nentially, and the time constant and amplitude of the fast and slow components are represented as follows,

$$p(t) = p_+ \exp(-t/\tau_+) + p_- \exp(-t/\tau_-) \quad (6)$$

$$p_\pm = \frac{1}{2} \mp \frac{k_{-a} - k_a + k_b}{2\sqrt{(k_a + k_{-a} + k_b)^2 - 4k_a k_b}} \quad (7)$$

$$\tau_\pm = \frac{1}{2}(k_a + k_{-a} + k_b) \pm \frac{1}{2}\sqrt{(k_a + k_{-a} + k_b)^2 - 4k_a k_b} \quad (8)$$

where p_+ (p_-) and τ_+ (τ_-) correspond to the amplitude and the time constant for the fast (slow) relaxation component, respectively. Using these equations and the results of the biexponential fitting to the transient grating signal for the CCl_4 solution, the time constants for each step can be estimated as $1/k_a = 330$ fs, $1/k_{-a} = 660$ fs, and $1/k_b = 850$ fs. It should be noted that all three rate processes occur on subpicosecond time scales, which are much shorter than a typical time scale of energy transfer to the solvent from 10 to 100 ps. The transient grating signals observed for the CCl_4 and DMF solutions are indicative of a relaxation pathway independent of the solvent and the importance of the intramolecular process.

Let us discuss the nature of the intermediate states. A candidate for the intermediate state may be a combination of overtone bands of states which could be strongly coupled to the −N═C═N− antisymmetric stretching mode. The band at 2068 cm^{-1} observed in the IR spectrum might be the intermediate state. This state may be formed by a Fermi resonance between the −N═C═N− antisymmetric stretching mode and an overtone or a combination band of other intramolecular modes. There have been several reports on vibrational assignment on carbodiimide compounds including DCCD.[26,33−35] For some alkyl carbodiimide compounds the −N═C═N− symmetric stretching mode was assigned to appear around 1400−1500 cm^{-1}, and it is revealed from this study that it appears at 1407 cm^{-1} for DCCD. A combination band of this stretching mode and other modes with frequencies at around 600−700 cm^{-1} could be anharmonically coupled to the −N═C═N− antisymmetric stretching mode. According to the results of the DFT calculation the −N═C═N− bending mode has a frequency of about 590 cm^{-1}, however, a sum of frequencies of these modes (1407 + 590 = 1997 cm^{-1}) is slightly smaller than the frequency of the mode (∼2120 cm^{-1}). The mode with a frequency of 1407 cm^{-1} is not strictly localized at the cumulative double bond and the C−H bending motions also contribute to it. The modes related bending motion may be able to couple to the −N═C═N− antisymmetric stretch. A band at 1078 cm^{-1} in the IR spectrum of DCCD was previously assigned as the C−N stretching mode,[26] though it is not confirmed by the present DFT calculation. The overtone of this mode might be this state. A two-color IR pump−probe technique will be useful in revealing the accepting modes of the −N═C═N− antisymmetric stretching mode of DCCD after the excitation of the N═C═N antisymmetric stretching mode.

V. Summary

The vibrational population relaxation of the carbodiimide (−N═C═N−) antisymmetric stretching mode of dicyclohexylcarbodiimide (DCCD) has been investigated by the transient grating method with femtosecond IR pulses. The transient grating signal shows nonexponential decay and is fitted well with a square of a biexponential function with time constants of about 200−300 fs and 1.4−1.5 ps. By frequency-resolving the signal we found that this nonexponentiality results from population relaxation on the $v = 1$ state. The biexponential population relaxations on the $v = 1$ state may be caused by rapid population distribution with nearby states and the irreversible relaxation. Currently, photon echo experiments on this vibrational mode are under progress to study vibirational dephasing.[31]

Acknowledgment. This work was supported by a Grant-In-Aid (10206101, 12304036, 13554019) from the Ministry of Education, Science, Sports, and Culture, and a JSPS research grant for the Future Program. Financial support from the Sumitomo Foundation, the Shimadzu Science Foundation, and the Kurata Foundation is also acknowledged. K.O. was supported by a fellowship from the Japan Society of Promotion for Science for Young Scientists. We are grateful to Prof. Yasuhisa Mizutani and Prof. Shinji Saito for valuable discussions.

References and Notes

(1) Fendt, A.; Fischer, S. F.; Kaiser, W. *Chem. Phys.* **1981**, *57*, 55.
(2) Zinth, W.; Kolmeder, C.; Benna, B.; Defregger, A. I.; Fischer, S. F.; Kaiser, W. *J. Chem. Phys* **1983**, *78*, 3916.
(3) Wang, Z.; Pakoulev, A.; Dlott, D. D. *Science* **2002**, *296*, 2201.
(4) Iwaki, L. K.; Dlott, D. D. *Chem. Phys. Lett.* **2000**, *321*, 419.
(5) Laenen, R.; Simeonidis, K.; Laubereau, A. *J. Phys. Chem. B* **2002**, *106*, 408.
(6) Kropman, M. F.; Bakker, H. J. *Chem. Phys. Lett.* **2003**, *370*, 741.
(7) Oxtoby, D. W. *Annu. Rev. Phys. Chem.* **1981**, *32*, 77.
(8) Owrutsky, J. C.; Raftery, D.; Hochstrasser, R. M. *Annu. Rev. Phys. Chem.* **1994**, *45*, 519.
(9) Hamm, P.; Lim, M.; Hochstrasser, R. M. *J. Phys. Chem. B* **1998**, *102*, 6123.
(10) Zanni, M. T.; Asplund, M. C.; Hochstrasser, R. M. *J. Chem. Phys.* **2001**, *114*, 4579.
(11) Lim, M.; Hochstrasser, R. M. *J. Chem. Phys.* **2001**, *115*, 7629.
(12) Hamm, P.; Lim, M.; Hochstrasser, R. M. *Phys. Rev. Lett.* **1998**, *81*, 5326.
(13) Rector, K. D.; Kwok, A. S.; Ferrante, C.; Tokmakoff, A.; Rella, C. W.; Fayer, M. D. *J. Chem. Phys.* **1997**, *106*, 10027.
(14) Clayden, J.; Greeves, N.; Warren, S.; Wothers, P. *Organic Chemistry*; Oxford University Press: New York, 2001.
(15) Kurzer, F.; Douraghi-Zadeh, K. *Chem. Rev.* **1967**, *67*, 107.
(16) Williams, A.; Ibrahim, I. T. *Chem. Rev.* **1981**, *81*, 589.
(17) Shimizu, T.; Seki, N.; Taka, H.; Kamigata, N. *J. Org. Chem.* **1996**, *61*, 6013.
(18) Schuster, E.; Hesse, C.; Schumann, D. *Synlett* **1991**, *12*, 916.
(19) Olah, G. A.; Wu, A.; Farooq, O. *Synthesis* **1989**, *7*, 568.
(20) Tahmassebi, D. *J. Chem. Soc., Perkin Trans. 2* **2001**, *4*, 613.
(21) Koput, J.; Jabs, W.; Winnewisser, M. *Chem. Phys. Lett.* **1998**, *295*, 462.
(22) Vincent, A. T.; Wheatley, P. J. *J. Chem. Soc., Perkin Trans. 2* **1972**, 687.
(23) Mukamel, S. *Principles of Nonlinear Optical Spectroscopy*; Oxford University Press: New York, 1995.
(24) Maekawa, H.; Tominaga, K.; Podenas, D. *Jpn. J. Appl. Phys.* **2002**, *41*, 329.
(25) Demirdöven, N.; Khalil, M.; Golonzka, O.; Tokmakoff, A. *Opt. Lett.* **2002**, *27*, 433.
(26) Ramaswamy, K.; Ranganathan, V.; Kambaram, E. *Acta Phys. Pol.* **1970**, *A38*, 839.
(27) Meakins, G. D.; Moss, R. J. *J. Chem. Soc.* **1957**, 993.
(28) Frisch, M. J.; Trucks, G. W.; Schlegel, H. B.; Scuseria, G. E.; Robb, M. A.; Cheeseman, J. R.; Montgomery, J. A., Jr.; Vreven, T.; Kudin, K. N.; Burant, J. C.; Millam, J. M.; Iyengar, S. S.; Tomasi, J.; Barone, V.; Mennucci, B.; Cossi, M.; Scalmani, G.; Rega, N.; Petersson, G. A.; Nakatsuji, H.; Hada, M.; Ehara, M.; Toyota, K.; Fukuda, R.; Hasegawa, J.; Ishida, M.; Nakajima, T.; Honda, Y.; Kitao, O.; Nakai, H.; Klene, M.; Li, X.; Knox, J. E.; Hratchian, H. P.; Cross, J. B.; Adamo, C.; Jaramillo, J.; Gomperts, R.; Stratmann, R. E.; Yazyev, O.; Austin, A. J.; Cammi, R.; Pomelli, C.; Ochterski, J. W.; Ayala, P. Y.; Morokuma, K.; Voth, G. A.; Salvador, P.; Dannenberg, J. J.; Zakrzewski, V. G.; Dapprich, S.; Daniels, A. D.; Strain, M. C.; Farkas, O.; Malick, D. K.; Rabuck, A. D.; Raghavachari, J. B.; Foresman, J. V.; Ortiz, J. V.; Chi, Q.; Baboul, A. G.; Clifford, S.; Cioslowski, J.; Stefanov, B. B.; Liu, G.; Liashenko, A.; Piskorz,

P.; Komaromi, I.; Martin, R. L.; Fox, D. J.; Keith, T.; Al-Laham, M. A.; Peng, C. Y.; Nanayakkara, A.; Challacombe, M.; Gill, P. M. W.; Johnson, B.; Chen, W.; Wong, M. W.; Gonzalez, G.; Pople, J. A. *Gaussian 03W*, Revision A.1; Gaussian, Inc.: Pittsburgh, PA, 2003.

(29) Fleming, G. R. *Chemical Applications of Ultrafast Spectroscopy*; Oxford University Press: New York, 1986.

(30) Asplund, M. C.; Lim, M.; Hochstrasser, R. M. *Chem. Phys. Lett.* **2000**, *323*, 269.

(31) Maekawa, H.; Ohta, K.; Tominaga, K. To be submitted for publication.

(32) Laenen, R.; Rauscher, C.; Laubereau, A. *Chem. Phys. Lett.* **1998**, *283*, 7.

(33) King, S. T.; Strope, J. H. *J. Chem. Phys.* **1971**, *54*, 1289.

(34) Ebsworth, E. A. V.; Mays, M. J. *Spectrochim. Acta* **1963**, *19*, 1127.

(35) Cradock, S.; Ebsworth, E. A. V. *J. Chem. Soc. A* **1968**, 1423.